AEM
Journals.ASM.org

Spatial Patterns of Carbonate Biomineralization in Biofilms

Xiaobao Li,[a] David L. Chopp,[b] William A. Russin,[c] Paul T. Brannon,[c] Matthew R. Parsek,[d] Aaron I. Packman[a]

Department of Civil and Environmental Engineering, Northwestern University, Evanston, Illinois, USA[a]; Department of Engineering Sciences and Applied Mathematics, Northwestern University, Evanston, Illinois, USA[b]; Biological Imaging Facility, Northwestern University, Evanston, Illinois, USA[c]; Department of Microbiology, University of Washington, Seattle, Washington, USA[d]

Microbially catalyzed precipitation of carbonate minerals is an important process in diverse biological, geological, and engineered systems. However, the processes that regulate carbonate biomineralization and their impacts on biofilms are largely unexplored, mainly because of the inability of current methods to directly observe biomineralization within biofilms. Here, we present a method for *in situ*, real-time imaging of biomineralization in biofilms and use it to show that *Pseudomonas aeruginosa* biofilms produce morphologically distinct carbonate deposits that substantially modify biofilm structures. The patterns of carbonate biomineralization produced *in situ* were substantially different from those caused by accumulation of particles produced by abiotic precipitation. Contrary to the common expectation that mineral precipitation should occur at the biofilm surface, we found that biomineralization started at the base of the biofilm. The carbonate deposits grew over time, detaching biofilm-resident cells and deforming the biofilm morphology. These findings indicate that biomineralization is a general regulator of biofilm architecture and properties.

Microbially induced carbonate precipitation represents an essential pathway for sequestration of large amounts of carbon in ancient and modern environments (1–5). Rock records reveal that Precambrian stromatolites formed as a consequence of trapping, binding, and precipitation of calcium carbonate by the growth and metabolism of microorganisms (2–4). Modern carbonate microbialites are found in a wide range of environments, including freshwater, oceans, hypersaline lakes, and soils (6, 7). Clinically, prolonged bacterial infection of indwelling urinary catheters leads to the formation of mineralized biofilms that can occlude the catheter lumen and cause serious complications (8–10). Some persistent infections of the lungs, particularly those associated with the genetic disorder primary ciliary dyskinesia, involve precipitation of calcium-rich stones or coatings (11–14). In engineered systems, microbially induced scale formation decreases the performance of a wide variety of processes, including membrane separations in water treatment and heat exchange efficiency in cooling towers (15, 16). More recently, calcium carbonate biomineralization has also been explored as a novel biotechnology for the purpose of bioremediation and stabilization of porous structures, including soils, sediments, and construction materials (17–21).

The microorganisms involved in carbonate biomineralization cover nearly all classes, including bacteria, algae, and fungi (22–27). It has been reported that more than 200 soil bacteria, including *Pseudomonas* spp., *Bacillus subtilis*, and *Azotobacter* spp., are capable of inducing calcium carbonate precipitation (5). Diverse microbial metabolisms, such as photosynthesis, sulfate reduction, and urea hydrolysis, can induce carbonate precipitation by significantly changing the saturation state of calcium carbonate (28, 29). Microbial respiration produces CO_2, decreases pH, and increases carbonate mineral dissolution. These biological processes have been intensively studied at the cellular scale (23, 30, 31). However, it is still very difficult to ascertain the specific role of microorganisms in carbonate precipitation because little is known about the processes that regulate carbonate biomineralization in complex environments, such as biofilms (1, 11, 32).

Biomineralization commonly occurs in microbial mats or biofilms, which are heterogeneous, surface-attached aggregates of microbial cells (6, 33–35). Spatial patterns in microbial growth and metabolism both respond to and influence local chemical microenvironments, leading to extremely variable conditions in and around biofilms (35–37). Biofilm respiration and protein synthesis activities show spatial variations in response to oxygen availability (35). pH also varies dramatically in biofilms (38). Biofilm microenvironment heterogeneity should facilitate biomineralization because it is more likely to lead to local supersaturation within the biofilm. *Ex situ* studies suggest that the extracellular polymeric substances (EPS) produced by biofilms influence precipitation and regulate patterns of mineralization (30, 39, 40). Nucleation models predict a random distribution of crystals in biofilm EPS in the absence of internal chemical gradients (3). Current models for biomineralization in biofilms suggest that mineral precipitation primarily occurs at the biofilm surface (41, 42). However, these models have not been supported by *in situ* observations, as little information is available on spatial patterns of mineral formation in biofilms. Consequently, the mechanisms that regulate the initial precipitation and overall accumulation of these deposits in biofilms are not understood.

Biomineralization can alter essential biofilm properties, including detachment, permeability, community metabolism, mechanical strength, and susceptibility to antimicrobials. Prior studies have found that deposition of solid particles alters biofilm

Received 13 May 2015 **Accepted** 27 July 2015

Accepted manuscript posted online 14 August 2015

Citation Li X, Chopp DL, Russin WA, Brannon PT, Parsek MR, Packman AI. 2015. Spatial patterns of carbonate biomineralization in biofilms. Appl Environ Microbiol 81:7403–7410. doi:10.1128/AEM.01585-15.

Editor: H. Nojiri

Address correspondence to Aaron I. Packman, a-packman@northwestern.edu.

Supplemental material for this article may be found at http://dx.doi.org/10.1128/AEM.01585-15.

morphology (43, 44). It has been suggested that this process should increase biofilm resistance to biocides by reducing transport of solutes into and within biofilms (45), but this hypothesis has not been tested experimentally. Calcium carbonate precipitation has also been found to increase the rigidity and strength of aerobic granules, which are biofilm-like suspended aggregates of cells encased in a matrix (21). However, the mechanisms that regulate interactions between biomineralization and biofilm properties are poorly understood, mainly because current endpoint visualization methods do not support real-time observations of biomineralization and associated feedback on other biofilm processes.

Here, we present real-time visualizations of calcium carbonate biomineralization in *Pseudomonas aeruginosa* biofilms and assess the resulting changes in biofilm properties. We also compare patterns of biofilm morphology and mineral deposits resulting from *in situ* biomineralization and *ex situ* precipitation in order to differentiate microbially catalyzed biomineralization from accumulation of abiotically precipitated material in biofilms.

MATERIALS AND METHODS

Experimental systems, strains, and inoculation procedure. Biofilm growth and biomineralization were observed in a flow cell system that supports continuous culturing of biofilms under a user-controlled growth medium, as described previously (46, 47). *P. aeruginosa* PAO1 strains with constitutively expressed fluorescence were used to form biofilms in these experiments, because *P. aeruginosa* is the most intensively studied model organism for biofilm formation and *Pseudomonas* spp. have previously been found to induce calcite precipitation (5, 31, 48). PAO1-*gfp* was used in all experiments, with the exception that PAO1-*mCherry* was used in experiments involving calcein staining, because calcein and green fluorescent protein (GFP) have similar fluorescence properties (49).

Log-phase bacterial cell cultures were grown in tryptic soy broth (TSB) (Difco) and then diluted in 1% TSB to a final optical density at 600 nm (OD_{600}) of 0.01 for inoculation into the flow cell chamber. The inoculated bacteria were allowed to attach to the cover glass surface under stagnant conditions (no flow) for 1 h. A flow of 1% TSB was then continuously supplied to the flow cell chamber for 3 days at a flow rate of 10 ml/h.

Calcium carbonate biomineralization in biofilms. Stock solutions (0.5 M and 1 M) of $NaHCO_3$ (99.5 to 100.5%; Sigma-Aldrich) and $CaCl_2$ (>99%; Sigma-Aldrich) were filter sterilized with 0.2-μm cellulose acetate membrane filters before use. Three-day-old PAO1 biofilms grown as described previously were subjected to flowthrough of a saturated calcium carbonate solution containing 15 mM (each) $CaCl_2$ and $NaHCO_3$ in 1% TSB. This solution has a pH of 7.6 and a saturation index ($\log\Omega$) of 1.88 at room temperature (~22°C) {$\Omega = ([Ca^{2+}][CO_3^{2-}])/K_S$, where K_S is the calcite solubility product constant and $[Ca^{2+}]$ and $[CO_3^{2-}]$ are the concentrations of Ca^{2+} and CO_3^{2-} in solution}. $\log K_S = -8.46$ at 22°C under atmospheric partial pressure of carbon dioxide (pCO_2) (50). Because the growth medium was highly dilute and the calcium carbonate solution was highly oversaturated, the effect of organic ligands was neglected in the calculation of the saturation state. The saturated solution was pumped through the flow cell at the same flow rate used to grow the biofilms for 12 to 17 h at room temperature.

A series of experiments were performed with calcein staining to confirm the calcium content of mineral precipitates. In experiments with calcein staining of *in situ* biomineralization, the saturated calcium carbonate solution was introduced with 5 μg/ml calcein. Calcein-labeled abiotic precipitates were obtained by adding 5 μg/ml calcein to a mixture of 100 mM $CaCl_2$ and $NaHCO_3$. Calcein stock solution (10 mg/ml) was prepared and stored following established protocols (51).

Confocal imaging. *In situ* imaging was performed by confocal laser scanning microscopy (CLSM) (Leica TCS SP2) using a 63× oil objective. A 488-nm argon ion laser was employed to excite bacterial self-expressed fluorescence (GFP and mCherry). Mineral deposits were imaged by collecting the reflection of the excitation laser in a detection window of 483 to 493 nm. Biomass (fluorescence) and mineral deposit (reflectance) signals were obtained simultaneously. This approach is similar to an imaging method described previously (52). In experiments involving calcein staining, residual calcein was rinsed from the flow cell and biofilm before imaging by flowthrough of deionized (DI) water for 15 min.

Confocal Raman microscopy. The mineralogy of biomineralized deposits was determined by confocal Raman microscopy (Princeton Instrument TriVista CRS). Biofilms containing mineral deposits were rinsed for 12 h with DI water at the same flow rate used in the primary experiments to remove residual calcium and carbonate ions. The entire flow cell chamber was then dried in air. Following drying, the coverslip was carefully removed from the flow cell with a steel blade, and the material on the coverslip was subjected to Raman microscopy. All Raman spectra were recorded at room temperature with a charge-coupled-device (CCD) detector (liquid nitrogen cooled) and an optical microscope with a 100× objective and an argon ion laser at 514 nm. Spectrum scanning was performed at a range of 100 to 1,600 cm^{-1} Raman shift with an interval of 1.6 cm^{-1}. The spectra show the overall Raman shifts from the field of view. The resulting data were analyzed using Origin 8 software.

Image analysis. Biofilms and mineral deposits were visualized and quantitatively compared using the Volocity software package (PerkinElmer, Inc.). Particle analysis was performed in ImageJ. Images were first transformed into binary format with appropriate thresholding, and then the area of each particle was measured by the Particle Analysis function in ImageJ. The biofilm biomass was quantified using the BioSPA (Biofilm Spatial Pattern Analysis) software package running in Matlab.

Biofilm detachment during biomineralization. Cell detachment from biofilms during biomineralization was monitored by enumerating CFU in the flow cell effluent. Effluent samples were collected at 1 and 2 h prior to the introduction of the biomineralization medium. After the introduction of the biomineralization medium, effluent samples were collected at 0, 1, 3, 4, 5, and 17 h. Effluent samples were vortexed to fully disperse the cells before plating. Cell detachment experiments were also conducted in nontreated biofilms or biofilms treated separately with $CaCl_2$ or $NaHCO_3$.

RESULTS

The deposition and precipitation of calcium carbonate in *P. aeruginosa* PAO1 biofilms were imaged within a flow cell by means of confocal microscopy. Biofilm morphology was imaged with the constitutively expressed GFP. PAO1 biofilms were grown under typical (nonbiomineralizing) conditions, yielding typical mushroom-shaped microcolonies surrounded by flat lawns of cells. These biofilms were then subjected to a supersaturated calcium carbonate medium to induce biomineralization within the biofilm. We confirmed that this medium was nontoxic to planktonic and biofilm-resident PAO1 cells (see Fig. S1 in the supplemental material).

We imaged the resulting deposits using the laser reflectance signal of confocal microscopy. Biomineralized deposits yielded a distinctive reflection signal (Fig. 1a). Mineral deposits imaged by the reflection signal showed irregular geometries that complemented voids in the biofilm (Fig. 1a and b). Annular patterns were observed in larger mineral deposits (Fig. 1a) because reflection occurred at the surfaces of the deposits. This allowed the outlines of the mineral deposits to be identified in each focal plane.

To verify that the reflection signal specifically identified calcium carbonate deposits, we labeled the deposits with calcein, a fluorophore that specifically binds to calcium (51, 53). Calcein specifically labeled abiotically precipitated and biomineralized calcium carbonate (Fig. 1; see Fig. S2 in the supplemental mate-

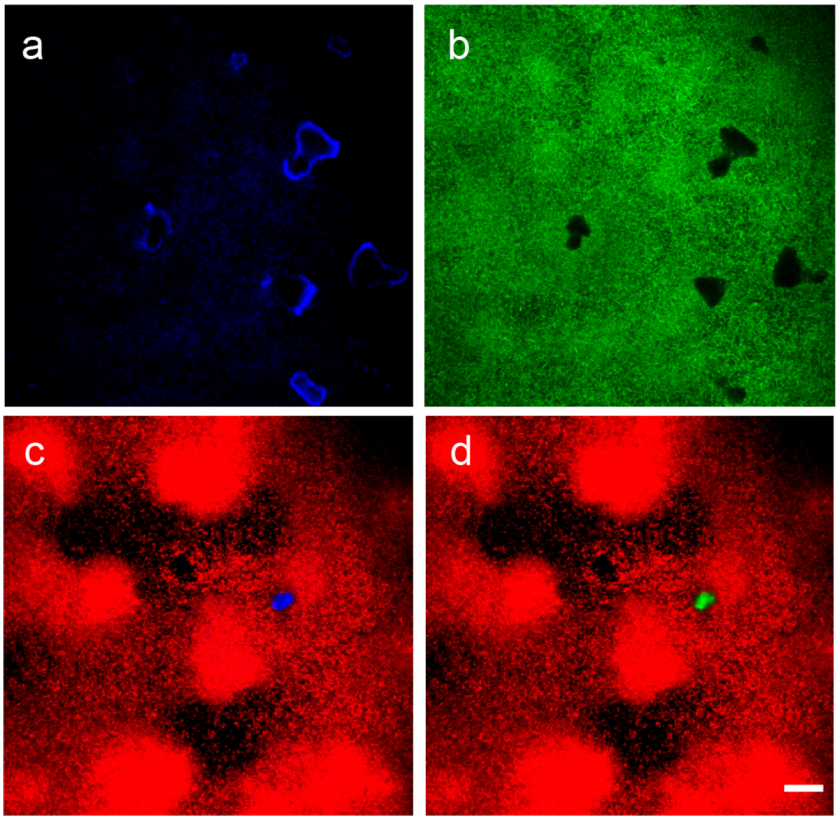

FIG 1 Imaging of mineral deposits in *P. aeruginosa* biofilms by confocal laser reflection. Calcium carbonate minerals and biofilm morphology were imaged simultaneously in PAO1-*gfp* (a and b) and PAO1-*mCherry* (c and d) biofilms. (a, c, and d) Minerals imaged by laser reflection appear blue (a and c), and those imaged by calcein staining appear green (d). (b, c, and d) Biomass appears green (PAO1-*gfp*) (b) and red (PAO1-*mCherry*) (c and d). (c and d) Minerals imaged by laser reflection and calcein staining present identical morphologies. Scale bar = 20 μm.

rial). Signals of carbonate deposits obtained by laser reflection and calcein emission also displayed good coincidence for both abiotic and biotic precipitates (Fig. 1c and d; see Fig. S2 in the supplemental material). Intensity-based Pearson's colocalization analysis (54) of the biotic-precipitate signals from laser reflection and calcein emission generated a relatively high colocalization coefficient (r_p) of 0.756.

In separate experiments, we confirmed the mineralogy of the biomineralized precipitates using confocal Raman microscopy. The spectra of biofilms containing biomineralized precipitates

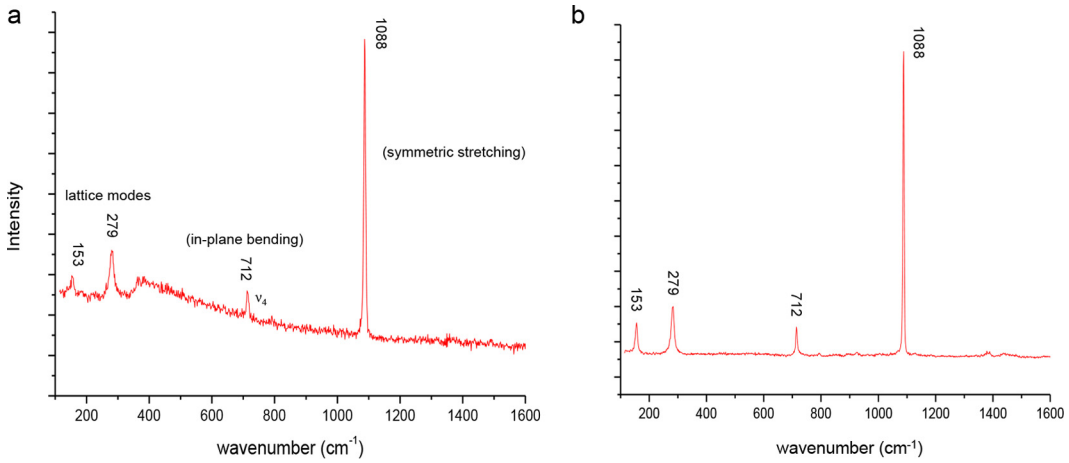

FIG 2 Panel a shows a Raman spectrum of biomineralized calcium carbonate minerals in a *P. aeruginosa* biofilm. The highest Raman shift intensity appears at 1,088 cm^{-1}, indicating the presence of carbonate minerals. The primary peaks match those in a calcite standard spectrum (shown in panel b), indicating that the biomineralized deposits are calcite and not aragonite.

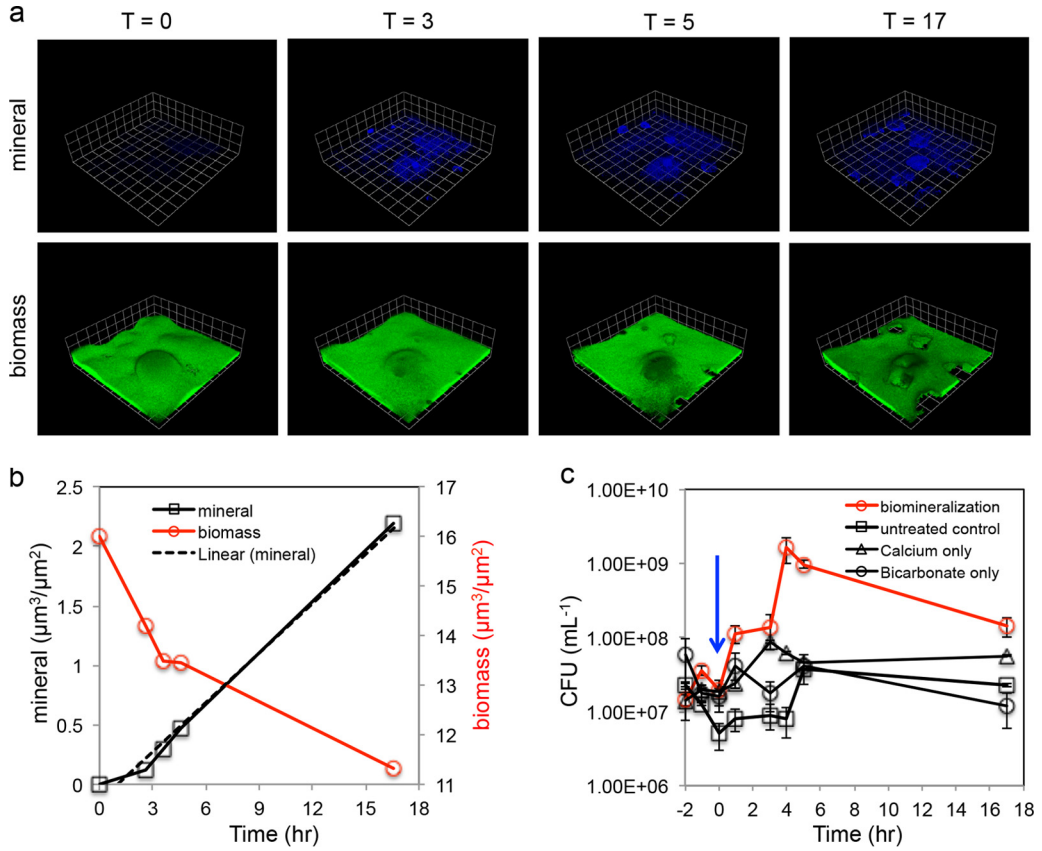

FIG 3 (a) Time series visualization of mineral growth and biofilm morphology. The same field of view was imaged at 0, 3, 5, and 17 h. Scale grid = 23 μm. See Fig. S4 in the supplemental material for orthogonal images. (b) Quantified biomass and mineral deposits in the field of view show opposite trends during biomineralization. (c) Detachment of cells from the biofilm during biomineralization. The cell concentration in the flow cell effluent was monitored for 2 h before biomineralization. Biomineralization medium or control treatments were introduced at t_0 (arrow). Cell counts in the flow cell effluent significantly increased during biomineralization, indicating that biomineralization induced detachment of cells from the biofilm. Increased cell detachment was not observed in biofilms under control conditions, including untreated biofilms and biofilms treated with 20 mM $CaCl_2$ or 20 mM $NaHCO_3$.

closely matched calcite standards (Fig. 2). The most prominent feature in the spectra of the biomineralized deposits is the peak at 1,088 cm^{-1}, which is from the internal vibrations (symmetric stretch) of the carbonate ion. In addition, the spectra show the calcite in-plane bending peak at 712 cm^{-1} and the lattice mode peak at 153 cm^{-1}. Similar bacterially induced calcite formation has been reported in a variety of natural and laboratory settings (5, 31, 55). Aragonite, which is another commonly observed microbially produced $CaCO_3$ mineral (1, 56, 57), has doublet bands at 701 cm^{-1} and 705 cm^{-1} from in-plane bending and the lattice mode peak at 205 cm^{-1} (58), but these features were absent in the spectra observed here. The deposits identified by reflectance also completely dissolved following a 15-min treatment with 0.01 M HCl, as expected for calcium carbonate (see Fig. S3 in the supplemental material).

These results indicate that the reflection signal specifically identified biomineralized calcite deposits within biofilms. Because the reflection method is noninvasive, it is suitable for real-time quantitative analysis of biomineralization processes within biofilms. While calcein also successfully labeled precipitated calcium carbonate in biofilms, it proved less suitable for quantitatively assessing *in situ* biomineralization because high concentrations of calcein increased the rate of calcium carbonate precipitation (presumably because of its strong binding of Ca^{2+}). Conversely, post-experiment staining with calcein did not yield a detectable signal of the precipitated deposits (results not shown).

We used the reflectance imaging method to observe spatiotemporal patterns of carbonate biomineralization within biofilms. We found that calcium carbonate biomineralization started from the base of the biofilm and the precipitated deposits expanded over time (Fig. 3a; see Fig. S4 in the supplemental material). Biomineralized deposits expanded from the initial nucleation sites and did not form at other locations in the biofilm, indicating that the initial deposits became preferential sites for further precipitation. The volume of the precipitated deposits increased linearly over time ($r^2 = 0.99$), and these deposits displaced an equivalent volume of biofilm biomass (Fig. 3b). This caused significant detachment of cells from the biofilm (Fig. 3c). Cell concentrations in the flow cell effluent were similar under all conditions and were at a magnitude of 10^7 CFU/ml (Fig. 3c). The number of CFU in the flow cell effluent significantly increased in biofilms under biomineralization treatment (Fig. 3c). Especially at 4 h, the cell concentration in the effluent reached 10^9 CFU/ml, which was 2 orders of magnitude higher than that before biomineralization. Such enhanced cell detachment was not observed in control experiments

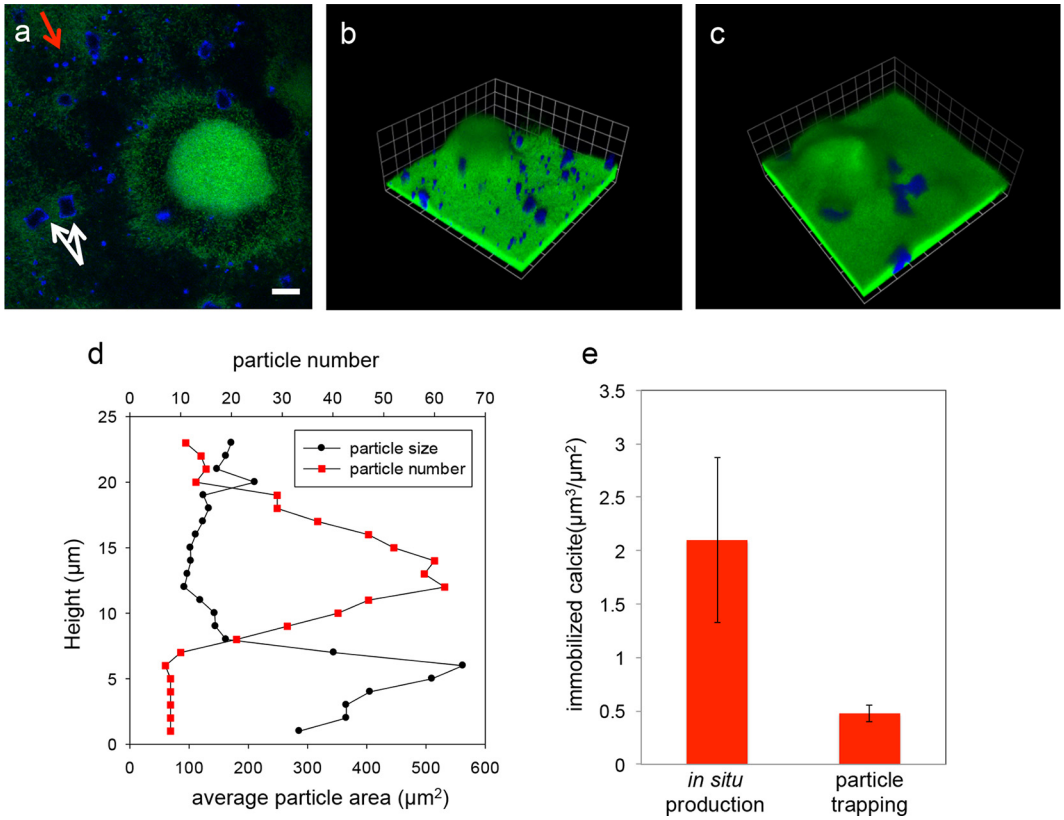

FIG 4 Spatial patterns of *in situ* calcite biomineralization and deposited calcite particles in *P. aeruginosa* biofilms. (a and b) Horizontal section (a) and three-dimensional (3D) rendering (b) of simultaneous *in situ* calcite biomineralization and deposition of abiotically precipitated calcite particles. (a) The red arrow indicates particles trapped on the biofilm surface, while the white arrows indicate deposits produced by *in situ* biomineralization. (c) When experiments were repeated with the flow cells inverted, no particles were deposited onto the biofilm surface, and only *in situ* biomineralization was observed. (d) Spatial patterns of mineral particle size over the depth of the biofilm. Biomineralization occurred at the base of the biofilm and produced larger deposits, while abiotic particles were smaller and were deposited at the biofilm surface. (e) The total volume of biomineralized deposits produced *in situ* was about four times greater than the volume of deposited calcite particles. The error bars were calculated from triplicate data sets from independent biomineralization experiments. Scale bar = 20 μm. Scale grid = 23 μm.

with nontreated biofilms or biofilms treated separately with $CaCl_2$ or $NaHCO_3$ (Fig. 3c), confirming that biomineralization was responsible for the observed cell detachment from biofilms.

Biomineralization did not occur in dead or metabolically inert biofilms under the same medium, indicating that the biomineralization process resulted from active cellular metabolism (see Fig. S5 in the supplemental material). Further, the process was localized within the biofilm, as the bulk pH did not change significantly during biomineralization (see Fig. S6 in the supplemental material). These results indicate that *in situ* biofilm metabolism actively regulates local microenvironments to facilitate carbonate precipitation within biofilms.

We compared patterns of *in situ* biomineralization with patterns of accumulation of calcium carbonate particles precipitated abiotically in solution. *In situ* biomineralization produced substantially larger deposits, different patterns of deposits, and more overall carbonate accumulation than abiotic precipitation (Fig. 4). *In situ* biomineralization yielded four times greater calcite accumulation in the biofilm than deposition of abiotically precipitated particles (Fig. 4e). Further, abiotic particles deposited only at the biofilm surface, while biomineralized deposits were larger and grew from the base of the biofilm (Fig. 4a, b, and d). Calcite deposits on the biofilm surface were similar in size to suspended particles (Table 1), indicating that these deposits originated from the bulk flow and did not precipitate *in situ*. We confirmed that these surficial deposits formed by gravitational settling of preprecipitated particles by repeating experiments with the flow cells inverted. In inverted flow cells, abiotic calcite particles did not deposit on the biofilm surface, confirming that the surficial deposits formed by gravitational settling, but biomineralization still occurred at the base of the biofilm, confirming that metabolism produces distinct patterns of biomineralization *in situ* (Fig. 4c).

TABLE 1 Sizes of calcite particles in different regions of flow cells containing *P. aeruginosa* biofilm

Particle source	Particle area (μm²) (mean ± SD)[a]
Flow cell inlet	47.2 ± 32.8
Precipitates deposited on biofilm surface	42.9 ± 15.7
Flow cell outlet	38.6 ± 18.2
In situ biomineralization	564 ± 110

[a] The means and standard deviations of 9 independent measurements are reported. The cross-sectional particle area was measured in ImageJ.

DISCUSSION

We developed a confocal imaging method for noninvasive, real-time visualization of biomineralization in biofilms and demonstrated that this method successfully resolved spatiotemporal patterns of calcium carbonate biomineralization. This method should also be suitable for imaging biomineralized deposits produced by other mechanisms, including ureolytic, photosynthetic, and sulfate reduction metabolisms.

We showed that *P. aeruginosa* biofilms induce substantial *in situ* precipitation of calcite and that the deposits produced by this mechanism are morphologically distinct from abiotically precipitated calcium carbonate particles (Fig. 4). There is an ongoing debate about the role of microbial processes in calcium carbonate precipitation in oversaturated environments, because the observed mineralization could simply be interpreted as a result of passive trapping and deposition of abiotic precipitates (1). Our results clarify that *in situ* biomineralization and trapping of abiotically precipitated particles occur simultaneously in biofilms under supersaturated conditions. Both processes immobilize inorganic carbon and contribute to microbial carbonate sequestration (59). In the experiments described here, *in situ* biomineralization was a more efficient carbonate sequestration pathway (Fig. 4e). In general, the relative importance of microbial and abiotic precipitation processes should be regulated by a combination of the saturation state of $CaCO_3$, local environmental conditions around biofilms, and native biofilm physiology.

The *in situ* observations presented here show that calcite precipitation is highly heterogeneous in biofilms. We expected to find such heterogeneity in biomineralization because biofilms are known to exhibit diverse and highly structured microenvironments resulting from a combination of microbial metabolism and transport limitations (35). Based on prior theoretical predictions (41, 42), we also expected biomineralization to occur primarily at the biofilm surface, but we observed strikingly different patterns of biomineralization *in situ*, with precipitation starting at the base of the biofilm and building upward (Fig. 3). The time series observations of spatial patterns in biomineralization we present here, therefore, challenge conventional biofilm models and suggest that *in situ* microbial processes, rather than delivery of ions from the bulk fluid, primarily regulate biomineralization in biofilms. Similar mineral distribution patterns have also been reported in calcium-rich aerobic granules (21).

We also found that the biomineralization process required active cellular metabolism (see Fig. S5 in the supplemental material). The most likely mechanisms for active calcite precipitation by *P. aeruginosa* are local accumulation of carbonate through cation transport and aerobic respiration and associated alteration of local pH microenvironments in regions of high cellular metabolism. Determination of the exact mechanism will require the development of new methods for direct, noninvasive observation of distributions of calcium and carbonate ions within biofilms to evaluate patterns of local supersaturation relative to cell density and metabolism.

Biofilm EPS can accumulate cations through sorption and provide initial crystallization sites for biomineralization (30, 39). However, it is difficult to ascertain the *in situ* functions of biofilm EPS matrix in calcite biomineralization. We found that no carbonate biomineralization occurred in the EPS mutant strain PAO1 Δ*pel* Δ*psl*, suggesting that biofilm EPS is important to carbonate precipitation. However, this conclusion is not definitive for EPS, because the mutant also exhibits significant deficiency in forming structured biofilms under flow (see Fig. S7 in the supplemental material). We also did not observe a clear correlation between EPS density and biomineralization patterns in PAO1 biofilms (see Fig. S8 in the supplemental material). Since calcite biomineralization was not found in metabolically inert biofilms (see Fig. S5 in the supplemental material) that still have the intact EPS matrix, we conclude that active metabolism, rather than EPS binding, is the predominant mechanism for heterogeneous carbonate biomineralization in biofilms.

Biofilm morphology affects external and internal solute transport patterns and therefore regulates the physiology of biofilm-resident cells (35, 60). Cell detachment also regulates biofilm physiology by controlling the organisms that are retained in the biofilm (61, 62). We showed that biomineralization causes detachment of biofilm-resident cells and alters biofilm morphology (Fig. 3), which indicates that biomineralization is a general regulator of biofilm physiology. Similar processes are expected to be important in diverse natural environments, engineered systems, and human infections, but limited understanding of biofilm physiology and chemodynamics makes it difficult to interpret specific mechanisms and outcomes of biomineralization in different settings. The methods presented here provide new tools for resolving biomineralization dynamics *in situ* and can be combined with other emerging imaging tools, such as fluorescently labeled chemical tracers and genetically engineered bioreporter strains, to provide new insight into coupled biophysicochemical controls on mineral precipitation.

This study provides the first direct *in situ* observations of calcite biomineralization by *P. aeruginosa* biofilms. *P. aeruginosa* is a ubiquitous organism in aquatic environments and also an important opportunistic pathogen (63). The results presented here show that *P. aeruginosa* biofilms can be used as a model system for investigations of calcite biomineralization. This is useful, because *P. aeruginosa* is a definitive model organism for biofilm studies (64), with numerous mutant and reporter strains available for experimentation.

Overall, our findings provide detailed information on spatial patterns of biomineralization in biofilms relevant to a diverse array of poorly understood problems, including microbial carbon sequestration, identification of biological signatures in the rock record, formation of harmful renal and urinary calculi, and microbial pulmonary calcification. The imaging method presented here can be broadly applied in conjunction with existing fluorescent imaging methods to assess feedback between biomineralization and other basic biofilm processes, including nutrient and substrate delivery, metabolic heterogeneity, antimicrobial susceptibility, and mechanical stability.

ACKNOWLEDGMENTS

We thank Yang Bai for helping to perform experiments and Jisun Song for commenting on an initial draft of the manuscript.

This work was supported by grant R01AI081983 from the National Institute of Allergy and Infectious Diseases, National Institutes of Health. Imaging analysis was performed at the Northwestern Biological Imaging Facility (BIF). Raman analysis was performed in the Keck-II facility at Northwestern University's Atomic and Nanoscale Characterization Experimental Center (NU*ANCE*). The NU*ANCE* Center is supported by the International Institute for Nanotechnology, MRSEC (NSF DMR-

1121262), the Keck Foundation, the State of Illinois, and Northwestern University.

X.L. and A.I.P. conceived the project and designed studies. X.L. performed experimental measurements. X.L., W.A.R., P.T.B., and A.I.P. developed the imaging methods. D.L.C developed the numerical model for diffusion analysis. X.L. and D.L.C performed image and data analysis. M.R.P. constructed strains. X.L. and A.I.P. wrote the paper. All authors discussed the results and commented on the manuscript.

REFERENCES

1. **Benzerara K, Menguy N, Lopez-Garcia P, Yoon TH, Kazmierczak J, Tyliszczak T, Guyot F, Brown GE.** 2006. Nanoscale detection of organic signatures in carbonate microbialites. Proc Natl Acad Sci U S A **103:**9440–9445. http://dx.doi.org/10.1073/pnas.0603255103.
2. **Grotzinger JP, Knoll AH.** 1999. Stromatolites in Precambrian carbonates: evolutionary mileposts or environmental dipsticks? Annu Rev Earth Planet Sci **27:**313–358. http://dx.doi.org/10.1146/annurev.earth.27.1.313.
3. **Arp G, Reimer A, Reitner J.** 2001. Photosynthesis-induced biofilm calcification and calcium concentrations in phanerozoic oceans. Science **292:**1701–1704. http://dx.doi.org/10.1126/science.1057204.
4. **Perri E, Spadafora A.** 2011. Evidence of microbial biomineralization in modern and ancient stromatolites. Stromatolites Interact Microbes Sediments **18:**633–649.
5. **Boquet E, Boronat A, Ramoscor A.** 1973. Production of calcite (calcium-carbonate) crystals by soil bacteria is a general phenomenon. Nature **246:**527–529. http://dx.doi.org/10.1038/246527a0.
6. **Dupraz C, Reid RP, Braissant O, Decho AW, Norman RS, Visscher PT.** 2009. Processes of carbonate precipitation in modern microbial mats. Earth Sci Rev **96:**141–162. http://dx.doi.org/10.1016/j.earscirev.2008.10.005.
7. **Sprachta S, Camoin G, Golubic S, Le Campion T.** 2001. Microbialites in a modern lagoonal environment: nature and distribution, Tikehau atoll (French Polynesia). Palaeogeogr Palaeoclimatol Palaeoecol **175:**103–124. http://dx.doi.org/10.1016/S0031-0182(01)00388-1.
8. **Stickler DJ.** 2008. Bacterial biofilms in patients with indwelling urinary catheters. Nat Clin Pract Urol **5:**598–608. http://dx.doi.org/10.1038/ncpuro1231.
9. **Warren JW.** 2001. Catheter-associated urinary tract infections. Int J Antimicrob Agents **17:**299–303. http://dx.doi.org/10.1016/S0924-8579(00)00359-9.
10. **Jacobsen SM, Stickler DJ, Mobley HLT, Shirtliff ME.** 2008. Complicated catheter-associated urinary tract infections due to Escherichia coli and Proteus mirabilis. Clin Microbiol Rev **21:**26–59. http://dx.doi.org/10.1128/CMR.00019-07.
11. **Kennedy MP, Noone PG, Carson J, Molina PL, Ghio A, Zariwala MA, Minnix SL, Knowles MR.** 2007. Calcium stone lithoptysis in primary ciliary dyskinesia. Respir Med **101:**76–83. http://dx.doi.org/10.1016/j.rmed.2006.04.007.
12. **Hekimoglu K, Gundogdu S.** 2008. Early adolescent primary ciliary dyskinesia associated with broncholithiasis. Pediatr Pulmonol **43:**714–716. http://dx.doi.org/10.1002/ppul.20826.
13. **Knowles MR, Daniels LA, Davis SD, Zariwala MA, Leigh MW.** 2013. Primary ciliary dyskinesia. Recent advances in diagnostics, genetics, and characterization of clinical disease. Am J Respir Crit Care Med **188:**913–922. http://dx.doi.org/10.1164/rccm.201301-0059CI.
14. **Seo JB, Song KS, Lee JS, Goo JM, Kim HY, Song JW, Lee IS, Lim TH.** 2002. Broncholithiasis: review of the causes with radiologic-pathologic correlation. Radiographics **22:**S199–S213. http://dx.doi.org/10.1148/radiographics.22.suppl_1.g02oc07s199.
15. **Teng F, Guan YT, Zhu WP.** 2008. Effect of biofilm on cast iron pipe corrosion in drinking water distribution system: corrosion scales characterization and microbial community structure investigation. Corros Sci **50:**2816–2823. http://dx.doi.org/10.1016/j.corsci.2008.07.008.
16. **Mattilasandholm T, Wirtanen G.** 1992. Biofilm formation in the industry—a review. Food Rev Int **8:**573–603. http://dx.doi.org/10.1080/87559129209540953.
17. **Warren LA, Maurice PA, Parmar N, Ferris FG.** 2001. Microbially mediated calcium carbonate precipitation: implications for interpreting calcite precipitation and for solid-phase capture of inorganic contaminants. Geomicrobiol J **18:**93–115. http://dx.doi.org/10.1080/01490450151079833.
18. **Lauchnor EG, Schultz LN, Bugni S, Mitchell AC, Cunningham AB, Gerlach R.** 2013. Bacterially induced calcium carbonate precipitation and strontium coprecipitation in a porous media flow system. Environ Sci Technol **47:**1557–1564. http://dx.doi.org/10.1021/es304240y.
19. **Mitchell AC, Dideriksen K, Spangler LH, Cunningham AB, Gerlach R.** 2010. Microbially enhanced carbon capture and storage by mineral-trapping and solubility-trapping. Environ Sci Technol **44:**5270–5276. http://dx.doi.org/10.1021/es903270w.
20. **Whiffin VS, van Paassen LA, Harkes MP.** 2007. Microbial carbonate precipitation as a soil improvement technique. Geomicrobiol J **24:**417–423. http://dx.doi.org/10.1080/01490450701436505.
21. **Ren TT, Liu L, Sheng GP, Liu XW, Yu HQ, Zhang MC, Zhu JR.** 2008. Calcium spatial distribution in aerobic granules and its effects on granule structure, strength and bioactivity. Water Res **42:**3343–3352. http://dx.doi.org/10.1016/j.watres.2008.04.015.
22. **Rodriguez-Navarro C, Rodriguez-Gallego M, Ben Chekroun K, Gonzalez-Munoz MT.** 2003. Conservation of ornamental stone by *Myxococcus xanthus*-induced carbonate biomineralization. Appl Environ Microbiol **69:**2182–2193. http://dx.doi.org/10.1128/AEM.69.4.2182-2193.2003.
23. **Lian B, Hu QN, Chen J, Ji JF, Teng HH.** 2006. Carbonate biomineralization induced by soil bacterium *Bacillus megaterium*. Geochim Cosmochim Acta **70:**5522–5535. http://dx.doi.org/10.1016/j.gca.2006.08.044.
24. **Lopez-Garcia P, Kazmierczak J, Benzerara K, Kempe S, Guyot F, Moreira D.** 2005. Bacterial diversity and carbonate precipitation in the giant microbialites from the highly alkaline Lake Van, Turkey. Extremophiles **9:**263–274. http://dx.doi.org/10.1007/s00792-005-0457-0.
25. **Breitbart M, Hoare A, Nitti A, Siefert J, Haynes M, Dinsdale E, Edwards R, Souza V, Rohwer F, Hollander D.** 2009. Metagenomic and stable isotopic analyses of modern freshwater microbialites in Cuatro Ciénegas, Mexico. Environ Microbiol **11:**16–34. http://dx.doi.org/10.1111/j.1462-2920.2008.01725.x.
26. **Obst M, Dynes JJ, Lawrence JR, Swerhone GDW, Benzerara K, Karunakaran C, Kaznatcheev K, Tyliszczak T, Hitchcock AP.** 2009. Precipitation of amorphous $CaCO_3$ (aragonite-like) by cyanobacteria: A STXM study of the influence of EPS on the nucleation process. Geochim Cosmochim Acta **73:**4180–4198. http://dx.doi.org/10.1016/j.gca.2009.04.013.
27. **Hartley AM, House WA, Leadbeater BSC, Callow ME.** 1996. The use of microelectrodes to study the precipitation of calcite upon algal biofilms. J Colloid Interface Sci **183:**498–505. http://dx.doi.org/10.1006/jcis.1996.0573.
28. **Machel HG.** 2001. Bacterial and thermochemical sulfate reduction in diagenetic settings—old and new insights. Sediment Geol **140:**143–175. http://dx.doi.org/10.1016/S0037-0738(00)00176-7.
29. **Stanley SM.** 2006. Influence of seawater chemistry on biomineralization throughout phanerozoic time: paleontological and experimental evidence. Palaeogeogr Palaeoclimatol Palaeoecol **232:**214–236. http://dx.doi.org/10.1016/j.palaeo.2005.12.010.
30. **Ercole C, Cacchio P, Botta AL, Centi V, Lepidi A.** 2007. Bacterially induced mineralization of calcium carbonate: the role of exopolysaccharides and capsular polysaccharides. Microsc Microanal **13:**42–50. http://dx.doi.org/10.1017/S1431927607070122.
31. **Fujita Y, Ferris EG, Lawson RD, Colwell FS, Smith RW.** 2000. Calcium carbonate precipitation by ureolytic subsurface bacteria. Geomicrobiol J **17:**305–318.
32. **Reid RP, Visscher PT, Decho AW, Stolz JF, Bebout BM, Dupraz C, Macintyre LG, Paerl HW, Pinckney JL, Prufert-Bebout L, Steppe TF, DesMarais DJ.** 2000. The role of microbes in accretion, lamination and early lithification of modern marine stromatolites. Nature **406:**989–992. http://dx.doi.org/10.1038/35023158.
33. **Shiraishi F, Bissett A, de Beer D, Reimer A, Arp G.** 2008. Photosynthesis, respiration and exopolymer calcium-binding in biofilm calcification (Westerhfer and Deinschwanger Creek, Germany). Geomicrobiol J **25:**83–94. http://dx.doi.org/10.1080/01490450801934888.
34. **Wimpenny J, Manz W, Szewzyk U.** 2000. Heterogeneity in biofilms. FEMS Microbiol Rev **24:**661–671. http://dx.doi.org/10.1111/j.1574-6976.2000.tb00565.x.
35. **Stewart PS, Franklin MJ.** 2008. Physiological heterogeneity in biofilms. Nat Rev Microbiol **6:**199–210. http://dx.doi.org/10.1038/nrmicro1838.
36. **De Beer D, Stoodley P, Roe F, Lewandowski Z.** 1994. Effects of biofilm structures on oxygen distribution and mass-transport. Biotechnol Bioeng **43:**1131–1138. http://dx.doi.org/10.1002/bit.260431118.
37. **Ramsing NB, Kuhl M, Jorgensen BB.** 1993. Distribution of sulfate-reducing bacteria, O_2, and H_2S in photosynthetic biofilms determined by

oligonucleotide probes and microelectrodes. Appl Environ Microbiol **59:** 3840–3849.
38. **Hunter RC, Beveridge TJ.** 2005. Application of a pH-sensitive fluoroprobe (C-SNARF-4) for pH microenvironment analysis in *Pseudomonas aeruginosa* biofilms. Appl Environ Microbiol **71:**2501–2510. http://dx.doi.org/10.1128/AEM.71.5.2501-2510.2005.
39. **Giuffre AJ, Hamm LM, Han N, De Yoreo JJ, Dove PM.** 2013. Polysaccharide chemistry regulates kinetics of calcite nucleation through competition of interfacial energies. Proc Natl Acad Sci U S A **110:**9261–9266. http://dx.doi.org/10.1073/pnas.1222162110.
40. **Braissant O, Cailleau G, Dupraz C, Verrecchia AP.** 2003. Bacterially induced mineralization of calcium carbonate in terrestrial environments: the role of exopolysaccharides and amino acids. J Sediment Res **73:**485–490. http://dx.doi.org/10.1306/111302730485.
41. **Zhang T, Klapper I.** 2010. Mathematical model of biofilm induced calcite precipitation. Water Sci Technol **61:**2957–2964. http://dx.doi.org/10.2166/wst.2010.064.
42. **Zhang TY, Klapper I.** 2011. Mathematical model of the effect of electrodiffusion on biomineralization. Int J Non Linear Mech **46:**657–666. http://dx.doi.org/10.1016/j.ijnonlinmec.2010.12.008.
43. **Drury WJ, Characklis WG, Stewart PS.** 1993. Interactions of 1 μM latex-particles with *Pseudomonas aeruginosa* biofilms. Water Res **27:**1119–1126. http://dx.doi.org/10.1016/0043-1354(93)90003-Z.
44. **Bouwer EJ.** 1987. Theoretical investigation of particle deposition in biofilm systems. Water Res **21:**1489–1498. http://dx.doi.org/10.1016/0043-1354(87)90132-1.
45. **Srinivasan R, Stewart PS, Griebe T, Chen CI, Xu XM.** 1995. Biofilm parameters influencing biocide efficacy. Biotechnol Bioeng **46:**553–560. http://dx.doi.org/10.1002/bit.260460608.
46. **Christensen BB, Sternberg C, Andersen JB, Palmer RJ, Nielsen AT, Givskov M, Molin S.** 1999. Molecular tools for study of biofilm physiology. Biofilms **310:**20–42. http://dx.doi.org/10.1016/S0076-6879(99)10004-1.
47. **Tseng BS, Zhang W, Harrison JJ, Quach TP, Song JL, Penterman J, Singh PK, Chopp DL, Packman AI, Parsek MR.** 2013. The extracellular matrix protects *Pseudomonas aeruginosa* biofilms by limiting the penetration of tobramycin. Environ Microbiol **15:**2865–2878. http://dx.doi.org/10.1111/1462-2920.12155.
48. **Zamarreno DV, Inkpen R, May E.** 2009. Carbonate crystals precipitated by freshwater bacteria and their use as a limestone consolidant. Appl Environ Microbiol **75:**5981–5990. http://dx.doi.org/10.1128/AEM.02079-08.
49. **Zhao K, Tseng BS, Beckerman B, Jin F, Gibiansky ML, Harrison JJ, Luijten E, Parsek MR, Wong GCL.** 2013. Psl trails guide exploration and microcolony formation in *Pseudomonas aeruginosa* biofilms. Nature **497:**388–391. http://dx.doi.org/10.1038/nature12155.
50. **Plummer LN, Busenberg E.** 1982. The solubilities of calcite, aragonite and vaterite in CO_2-H_2O solutions between 0-degrees-C and 90-degrees-C, and an evaluation of the aqueous model for the system $CaCO_3$-CO_2-H_2O. Geochim Cosmochim Acta **46:**1011–1040. http://dx.doi.org/10.1016/0016-7037(82)90056-4.
51. **Tambutte E, Tambutte S, Segonds N, Zoccola D, Venn A, Erez J, Allemand D.** 2012. Calcein labelling and electrophysiology: insights on coral tissue permeability and calcification. Proc Biol Sci **279:**19–27. http://dx.doi.org/10.1098/rspb.2011.0733.
52. **Connolly J, Kaufman M, Rothman A, Gupta R, Redden G, Schuster M, Colwell F, Gerlach R.** 2013. Construction of two ureolytic model organisms for the study of microbially induced calcium carbonate precipitation. J Microbiol Methods **94:**290–299. http://dx.doi.org/10.1016/j.mimet.2013.06.028.
53. **Tucker BM.** 1957. Calcein as an indicator for the titration of calcium with ethylenediaminetetra-acetate. Analyst **82:**284–285. http://dx.doi.org/10.1039/an9578200284.
54. **Adler J, Parmryd I.** 2010. Quantifying colocalization by correlation: the Pearson correlation coefficient is superior to the Mander's overlap coefficient. Cytometry A **77A:**733–742. http://dx.doi.org/10.1002/cyto.a.20896.
55. **Morita RY.** 1980. Calcite precipitation by marine-bacteria. Geomicrobiol J **2:**63–82. http://dx.doi.org/10.1080/01490458009377751.
56. **Buczynski C, Chafetz HS.** 1991. Habit of bacterially induced precipitates of calcium-carbonate and the influence of medium viscosity on mineralogy. J Sediment Petrol **61:**226–233. http://dx.doi.org/10.1306/D42676DB-2B26-11D7-8648000102C1865D.
57. **Decho AW.** 2010. Overview of biopolymer-induced mineralization: what goes on in biofilms? Ecol Eng **36:**137–144. http://dx.doi.org/10.1016/j.ecoleng.2009.01.003.
58. **Wehrmeister U, Soldati AL, Jacob DE, Hager T, Hofmeister W.** 2010. Raman spectroscopy of synthetic, geological and biological vaterite: a Raman spectroscopic study. J Raman Spectrosc **41:**193–201.
59. **Riding R.** 2000. Microbial carbonates: the geological record of calcified bacterial-algal mats and biofilms. Sedimentology **47:**179–214. http://dx.doi.org/10.1046/j.1365-3091.2000.00003.x.
60. **Wuertz S, Bishop PL, Wilderer PA.** 2003. Biofilms in wastewater treatment: an interdisciplinary approach. IWA Publishing, London, United Kingdom.
61. **Hall-Stoodley L, Costerton JW, Stoodley P.** 2004. Bacterial biofilms: from the natural environment to infectious diseases. Nat Rev Microbiol **2:**95–108. http://dx.doi.org/10.1038/nrmicro821.
62. **Uppuluri P, Chaturvedi AK, Srinivasan A, Banerjee M, Ramasubramaniam AK, Kohler JR, Kadosh D, Lopez-Ribot JL.** 2010. Dispersion as an important step in the Candida albicans biofilm developmental cycle. PLoS Pathog **6:**e1000828. http://dx.doi.org/10.1371/journal.ppat.1000828.
63. **Costerton JW, Cheng KJ, Geesey GG, Ladd TI, Nickel JC, Dasgupta M, Marrie TJ.** 1987. Bacterial biofilms in nature and disease. Annu Rev Microbiol **41:**435–464. http://dx.doi.org/10.1146/annurev.mi.41.100187.002251.
64. **O'Toole G, Kaplan HB, Kolter R.** 2000. Biofilm formation as microbial development. Annu Rev Microbiol **54:**49–79. http://dx.doi.org/10.1146/annurev.micro.54.1.49.